Vertical profiling of atmospheric refractivity from ground-based GPS

Anthony R. Lowry

GPS Science/Technology Group, University Corporation for Atmospheric Research (UCAR), Boulder, Colorado.
Now at: Department of Physics, University of Colorado, Boulder CO 80309-0390, arlowry@himalaya.colorado.edu, Phone: 303 492 5141, Fax: 303 492 7935

Chris Rocken, Sergey V. Sokolovskiy

GPS Science/Technology Group, University Corporation for Atmospheric Research (UCAR), Boulder, Colorado.

Kenneth D. Anderson

SPAWAR/SYSCEN, San Diego, California.

Abstract. Atmospheric refractivity is typically estimated *in situ* from radiosonde measurements, which are expensive and may undersample the spatial and temporal variability of weather phenomena. We estimate refractivity structure near San Diego, California, using ray propagation models to fit measured GPS tropospheric delays in a least-squares metric. We evaluate the potential and the limitations of ground-based GPS measurements for characterizing atmospheric refractivity, and we compare refractivity structure estimated from GPS sensing with that measured by nearby radiosondes. The results suggest that ground-based GPS provides significant constraint of inhomogeneous atmospheric refractivity, despite certain fundamental limitations of ground-based measurements. Radiosondes typically are launched just a few times daily. Consequently, estimates of temporally and spatially varying refractivity that assimilate GPS delays could substantially improve over estimates using radiosonde data alone.

1. Introduction

Terrestrial propagation of radio waves at frequencies above 30 MHz is significantly affected by tropospheric refraction [*Hitney et al.*, 1985], especially when the source and/or receiver is near a coastline. A famous example of anomalous propagation occurred in India during World War II, when a 200 MHz radar (with an expected range of several hundred km) detected the Arabian coast some 2700 km away [*Freehafer*, 1951]. Similar effects are observed near the southern California coast by cell phone users in Los Angeles and San Diego who, instead of connecting with their local cell, sometimes connect with a remote cell up to 150 km away.

Knowledge of the refractive environment is crucially important to predict radar detection ranges or maximum microwave communication ranges. The mid-1970s witnessed a flurry of development of refractive effects assessment systems. One such, the Integrated Refractive Effects Prediction System [*Hitney and Richter*, 1976; *Baumgartner et al.*, 1983], was installed onboard all U.S. Navy aircraft carriers to support mission planning for radar, communication, and aircraft operations. Currently, such radio propagation analyses rely on *in situ* measurement of the local refractivity profile using radiosondes. Signal propagation is modeled assuming the refractive environment is homogeneous in both range and time. However, radiosonde measurements are expensive, and they may undersample the spatial and temporal variations in refractory phenomena, particularly near coastlines.

Copyright 2002 by the American Geophysical Union.

Paper number 2000RS002565.
0148-0227/11/2000RS002565$9.00

Anomalous radio propagation effects can also be detected directly from measurements of propagation delays or Doppler frequency shift of electromagnetic signals. For example, radio frequency refractivity of the atmospheres of Mars, Venus and the Earth has been estimated from measurements of occultation Doppler shift between orbiting satellites [e.g., *Fjeldbo and Eshleman*, 1968; *Fjeldbo et al.*, 1971; *Kursinski et al.*, 1997; *Rocken et al.*, 1997]. Such measurements provide remarkably accurate, high-resolution estimates of the vertical refractivity structure of the troposphere, but occultations sample too sparsely in time and space to adequately constrain lateral and temporal variations of refractivity at a particular locale.

Ground-based measurements are potentially more informative about space-time variations of refractivity in a particular region [*Zuffada et al.*, 1999], but analyses of ground-based sensing of atmospheric refractivity thus far have examined that potential largely based on simulated observations [*Gaikovich and Sumin*, 1986; *Azizov et al.*, 1998; *Zuffada et al.*, 1999]. Applications of ground-based refractivity profiling are comparatively few [*Vasilenko et al.*, 1986; *Azizov et al.*, 1998], and profiling from GPS measurements has not yet been documented, primarily because of an inherent limitation of the source-receiver geometry. Space-based occultation profiling, and ground-based profiling that uses rays arriving from negative elevation angles (e.g., profiling the atmosphere below a mountaintop), entails inversion of a well-posed Volterra (Abel) integral equation [*Fjeldbo and Eshleman*, 1965]. However, when the receiver altitude is near that of the ground horizon, the ray elevations are always positive, and the inverse problem is described by an ill-posed Fredholm integral equation of the first kind [*Gaikovich and Sumin*, 1986]. Ground-based refractivity profiling is further hampered by the need to develop instruments and algorithms that can accurately measure signal delay at the low satellite elevation angles ($< 5^o$) that convey most of the refractive information.

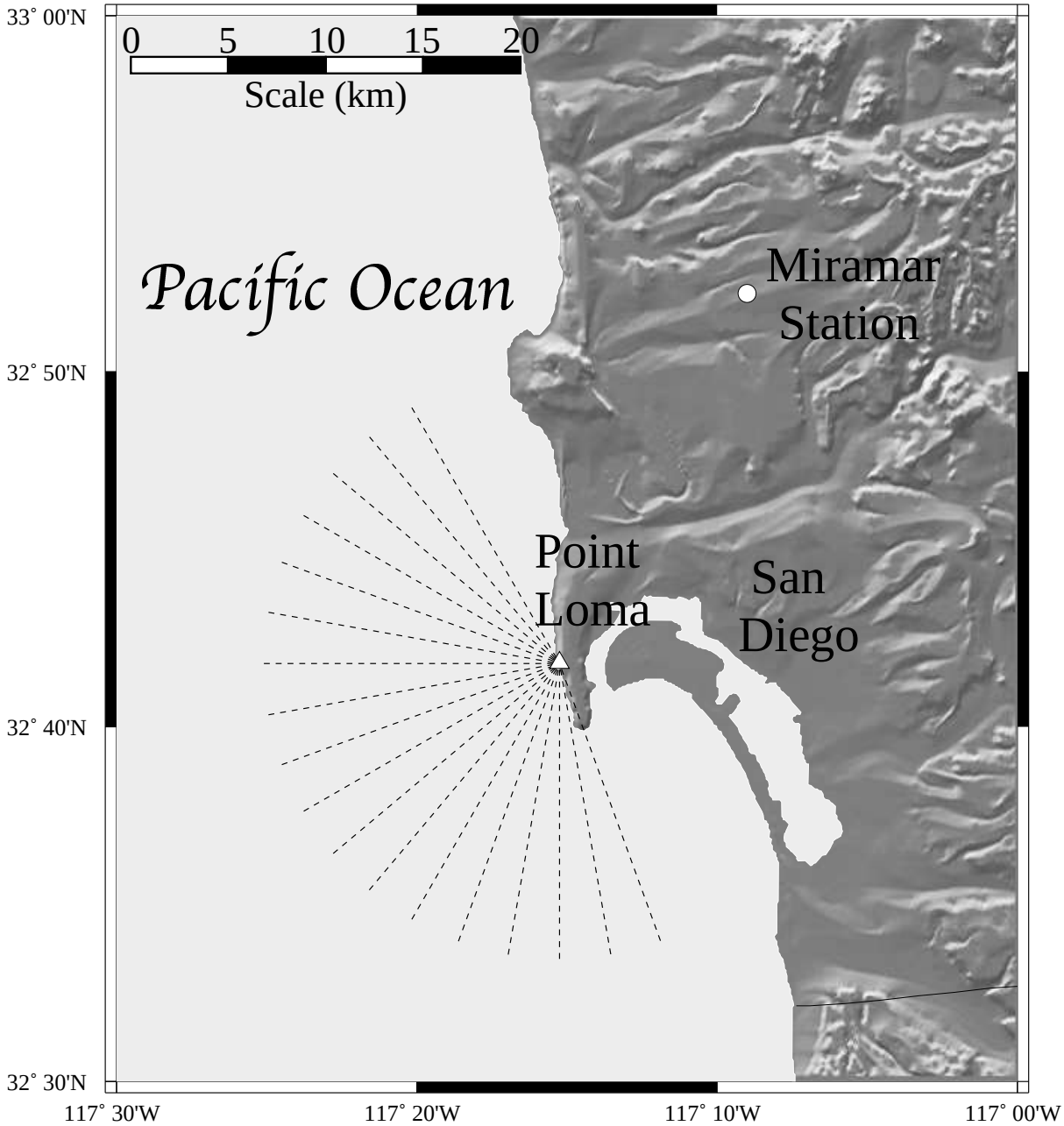

Figure 1. Location map of the study area near San Diego, California. The GPS receiver and Point Loma radiosonde release sites are indicated by the white triangle; radiosonde station Miramar is shown by the white circle. Dotted lines indicate azimuths along which GPS excess phase path was measured below 5° elevation.

In the following sections we examine vertical profiles of atmospheric refractivity estimated from GPS signal delay measured near San Diego, California, between October 19, 1999 and April 31, 2000. We evaluate the potential and the limitations of ground-based measurements of GPS delay for characterizing atmospheric refractivity, and we compare refractivity structure estimated from GPS with that measured by nearby radiosondes. The results are encouraging, and suggest that ground-based GPS provides significant constraint of inhomogeneous atmospheric refractivity.

2. GPS measurement of excess phase path

GPS data were collected from a pier overhanging the Pacific Ocean on Point Loma peninsula (Figure 1). Observables were recorded using an AOA SNR-8000 receiver retrofitted with Benchmark ACT^{TM} tracking. The receiver clock was steered by a Datum FTS1195 crystal oscillator, with 5×10^{-13} short-term stability. The antenna, a Dorne-Margolin (IGS standard) choke ring fitted with a special high-gain preamplifier, was tilted westward about 20° from horizontal to increase antenna gain for GPS satellites near the ocean horizon. Surface meteorological data were collected at 5 minute intervals by a Digiquartz Met3 sensor, located 12 m east of the GPS antenna. All data were logged onto a single personal computer onsite prior to being transferred to the University Corporation for Atmospheric Research (UCAR) in Boulder for analysis.

The observable we used to constrain refractivity was the excess phase path, i.e., the excess travel time between satellite and receiver that results from tropospheric bending and slowing, multiplied by the speed of light in vacuum [e.g., *Budden*, 1985]. GPS excess phase path was estimated using a modified version of Bernese v4.2 software [*Rothacher and Mervart*, 1996] in a precise point positioning

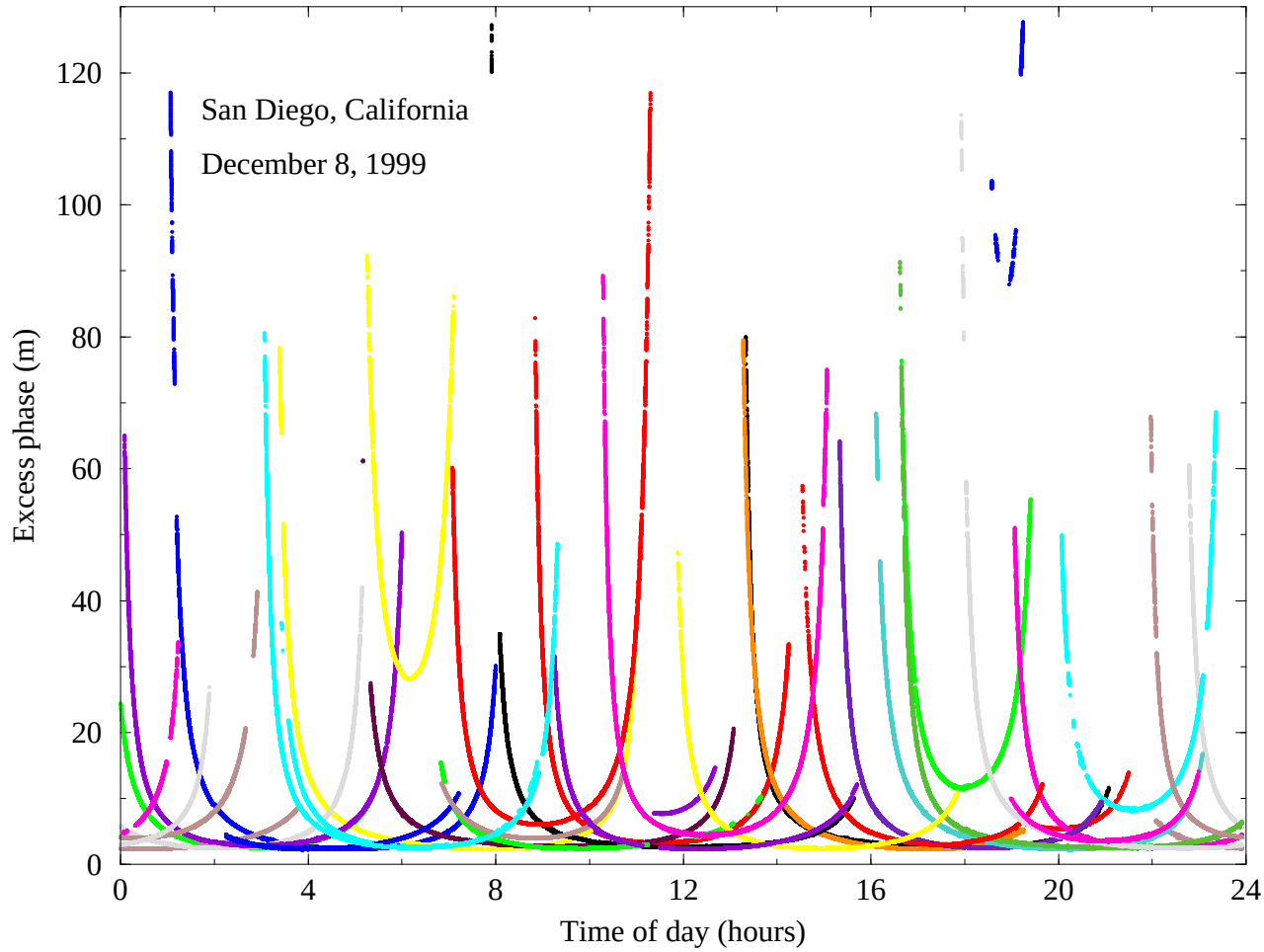

Figure 2. Measured excess phase path ΔS^{GPS} as a function of time on December 8, 1999.

mode [*Zumberge et al.*, 1997]. Precise point positioning requires precise ephemerides and high-rate satellite clock estimates; we used Jet Propulsion Laboratory (JPL) orbits and 1/30 Hz clock solutions [*Zumberge et al.*, 1998]. The GPS data were sampled at 1 Hz rates however, and so to process at 1 Hz we initially attempted to interpolate the 1/30 Hz satellite clocks. However, clock errors due to Selective Availability (SA) were aliased sufficiently by 1/30 Hz sampling to introduce significant errors in excess phase path (up to 30 cm after cubic spline interpolation). Consequently, we first estimated 1 Hz satellite clock rates using point positioning to the three nearest 1 Hz sites in the International GPS Service (IGS) global network (FAIR, KOKB, and GODE) using JPL orbits but ignoring the JPL clock solutions, and we then used the average of those clock rate estimates to interpolate the JPL 1/30 Hz clock solutions in processing of GPS data from Point Loma.

Only three parameters were estimated when processing the carrier phase and code GPS observables to get excess phase path: (1) the receiver clock error at each epoch, (2) the phase ambiguity, and (3) tropospheric wet zenith delay at half-hourly intervals, using *Niell*'s [1996] NMFH2 mapping function. Tropospheric dry delay was modeled from a modified *Hopfield* [1969] mapping of surface pressure and temperature measurements. Ionospheric dispersive delay was removed via the ionosphere-free linear combination of phase from the two GPS carrier frequencies [*Spilker*, 1978]. Data was weighted by the cosine of the zenith angle (and zero-weighted below 5° elevation) to minimize the impact of the simple tropospheric mapping functions on errors in other estimated parameters. The information that was retained after Bernese processing included (1) the position of the receiver, $\vec{r}_1$, which was fixed to an independent network solution rather than estimated, (2) the position and velocity of the GPS satellite, $\vec{r}_2(t)$ and $\vec{v}_2(t)$, derived from the precise ephemerides, and (3) the measured excess phase path ΔS^{GPS} (combining the dry delay model, estimated wet delay and the post-fit residual).

An example of measured excess phase path ΔS^{GPS} is shown in Figure 2. ΔS^{GPS} varies from $\sim$2 m at zenith to more than 100 m at low satellite elevation angles. Lowest elevation data are prone to gaps in observations, due partly to masking by structures and topography east of the instrument and partly to multipath cancellation. Reflections off the ocean surface generate strong multipath, and signal strength reduction by destructive interference commonly results in loss of L2 phase lock for satellites at low elevation [e.g., *Anderson*, 1994]. Most of the information about the vertical distribution of refractivity is contained at low satellite elevation angles less than $\sim 5^o$ [e.g., *Gaikovich and Sumin*, 1986], and of the 70 processed satellite rises and sets depicted in Figure 2, only 27 had usable observations at those elevations. On average, we collected 24 usable rises and sets per day over the course of the experiment.

3. Modeling of excess phase path

GPS excess phase path was modeled using an integral expression derived from ray theory. Assuming a spherical, radially symmetric refractive medium, a ray is described by Snell's law as [e.g., *Born and Wolf*, 1964]:

$$rn(r)\sin\alpha = a, \tag{1}$$

in which α is the angle of ray propagation from the vertical (zenith) direction (Figure 3), n is the refractive index, and a is a constant for

a given ray (termed the impact parameter, if the ray is not trapped). The phase path between points 1 and 2 on a ray is

$$S = \int_1^2 n(r)\mathrm{d}l \tag{2}$$

where $\mathrm{d}l = \sqrt{\mathrm{d}r^2 + r^2\mathrm{d}\theta^2}$ in polar coordinates. Substituting $\mathrm{d}r = \mathrm{d}l\cos\alpha$ and using Snell's law (1), equation (2) may be expressed as

$$S = \int_{r_1}^{r_2} \frac{rn^2(r)}{\sqrt{r^2n^2(r) - a^2}}\mathrm{d}r = \int_{x_1}^{x_2} \frac{[1 - \frac{x}{n}\frac{\mathrm{d}n}{\mathrm{d}x}]x}{\sqrt{x^2 - a^2}}\mathrm{d}x, \tag{3}$$

where $x \equiv rn(r)$ is the refractional radius. Equation (3) permits calculation of the phase path S for a given impact parameter, or for given zenith angle of the ray at a point r (unless the ray has a perigee point between 1 and 2, in which case (3) consists of separate terms describing the ray sections on either side). The excess phase path is simply $\Delta S = S - S_0$ (where S_0 is the path in vacuum, i.e., the distance between the antenna 1 and GPS satellite 2) and is a function of the elevation angle β of the straight line connecting 1 and 2. ΔS cannot be calculated explicitly for given β; rather, we calculate ΔS and β for a given impact parameter a using the bending angle ϵ of the ray connecting satellite and receiver:

$$\epsilon = \int_1^2 \frac{\mathrm{d}l}{\rho} \tag{4}$$

where ρ is the local radius of curvature of the ray. In polar coordinates,

$$\rho = \frac{\left[r^2 + \left(\frac{\mathrm{d}r}{\mathrm{d}\theta}\right)^2\right]^{3/2}}{r^2 + 2\left(\frac{\mathrm{d}r}{\mathrm{d}\theta}\right)^2 - r\left(\frac{\mathrm{d}^2r}{\mathrm{d}\theta^2}\right)}. \tag{5}$$

Substituting (5) into (4) and using Snell's law (1), the expression for ϵ is

$$\epsilon = -a\int_{r_1}^{r_2} \frac{\mathrm{d}n/\mathrm{d}r}{n(r)\sqrt{r^2n^2(r) - a^2}}\mathrm{d}r = -a\int_{x_1}^{x_2} \frac{\mathrm{d}n/\mathrm{d}x}{n(x)\sqrt{x^2 - a^2}}\mathrm{d}x. \tag{6}$$

Once S and ϵ are calculated, the spherical angle θ between points 1 and 2 is given by:

$$\theta = \arcsin\left[\frac{a}{x_1}\right] - \arcsin\left[\frac{a}{x_2}\right] + \epsilon \tag{7}$$

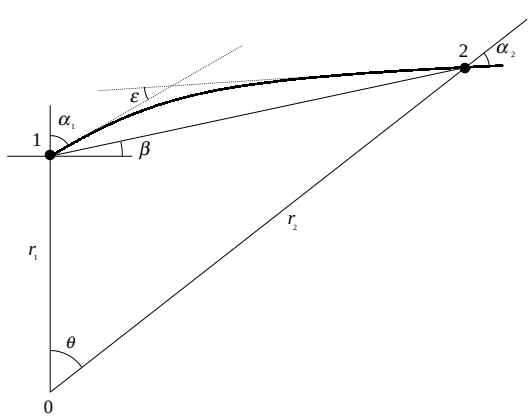

Figure 3. Graphical depiction of the geometric parameters of refractive bending.

The elevation angle β is then:

$$\beta = \arctan\left(\frac{r_2\cos\theta - r_1}{r_2\sin\theta}\right) \tag{8}$$

and the path in vacuum S_0:

$$S_0 = \sqrt{r_1^2 + r_2^2 - 2r_1r_2\cos\theta} \tag{9}$$

In practice, we defi ne the center of sphericity ($r = 0$) to be the local center of curvature of the reference ellipsoid at $\vec{r_1}$ in the direction of $\vec{r_2}$. Then we calculate ΔS and β on a dense mesh of impact parameters a and interpolate the discrete model of $\Delta S(\beta)$ to the β of our observations using cubic splines.

4. Parameter search for best fit model

To parameterize the GPS measurement of excess phase path $\Delta S^{\mathrm{GPS}}(\beta)$, we assume an array of refractivity models $N(r) = 10^6 \times [n(r) - 1]$, calculate for each a modeled excess phase path $\Delta S^{\mathrm{mod}}(\beta)$, and compare with the measured $\Delta S^{\mathrm{GPS}}(\beta)$ to determine which provides the best fi t in a least-squares sense. The model design was motivated partly by a desire to characterize anomalous refractivity gradients. Normally the vertical refractivity gradient is negative, $\mathrm{d}N/\mathrm{d}r < 0$, so that rays are bent toward the Earth's surface, and most often the radius of curvature of rays is greater than the Earth's radius r_E. However when the radius of ray curvature at a tangent point is equal to the spherical radius, i.e., $\mathrm{d}n/\mathrm{d}r = -n/r \simeq -160\ N\ \mathrm{km}^{-1}$, the ray is critically refracted, and when $\mathrm{d}n/\mathrm{d}z < -n/r$, it is referred to as super-refraction. Rays having tangent points within a super-refracting layer are trapped.

The refractivity model used here (Figure 4) consists of a constant normal gradient ($-10\ N$-units km^{-1}) beginning at the receiver altitude $Z_1 \equiv r_1 - r_E$, a critically refractive gradient ($-160\ N$-units km^{-1}) between altitudes Z_A and Z_B, and a constant gradient between Z_B and 6 km altitude. There are only two independent variable parameters in the model, corresponding to the altitudes Z_B and Z_A at top and bottom of the critically refractive gradient. Refractivity at the receiver, N_1, is calculated from pressure, temperature and relative humidity (P, T, ν) collected at the surface meteorological sensor. Refractivity is related to atmospheric parameters via [e.g.,

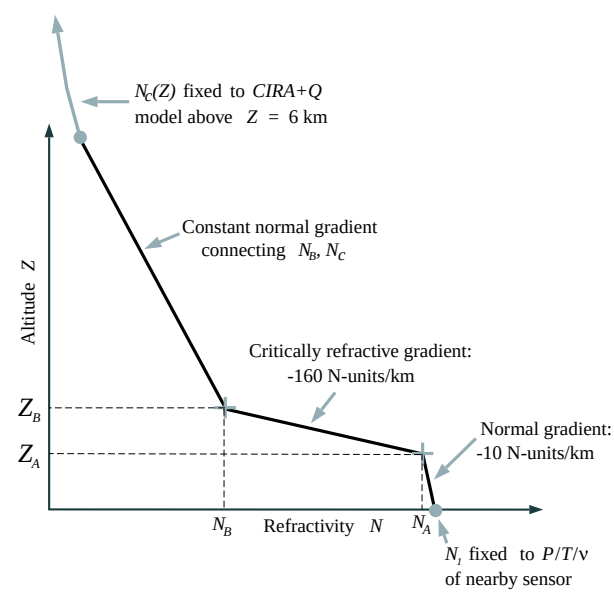

Figure 4. The refractivity model used in this analysis. Variable parameters are Z_A and Z_B.

Thayer, 1974]:

$$N = 77.6\frac{P_a Z_a^{-1}}{T} + \left(64.8 + \frac{3.776\times10^5}{T}\right)\frac{eZ_w^{-1}}{T} \quad (10)$$

in which $P_a = P - e$ is the partial pressure of dry air in hPa, e is the partial pressure of water vapor (obtained from percent relative humidity ν via):

$$e = 0.0611\nu \exp\left[\frac{17.67t}{T - 29.65}\right], \quad (11)$$

and the inverse compressibility constants Z_a^{-1} and Z_w^{-1} are approximated by [*Owens*, 1967]:

$$Z_a^{-1} = 1 + 57.9\times10^{-8}\left(1 + \frac{0.52}{T}\right)P_a - 9.4611\times10^{-4}\frac{tP_a}{T^2} \quad (12)$$

and

$$Z_w^{-1} = 1 + 1650\frac{e}{T^3}(1 - 0.01317t + 1.75^{-4}t^2 + 1.44\times10^{-6}t^3), \quad (13)$$

where T is temperature in ^{o}K and t in ^{o}C. Above 6 km the model uses refractivity from (P, T, ν) of the COSPAR International Reference Atmosphere including humidity (CIRA+Q) [*Kirchengast et al.*, 1999] and equations (10)–(13).

The model was skeletalized from refractivity structure observed in high-resolution radiosonde measurements collected near the site.

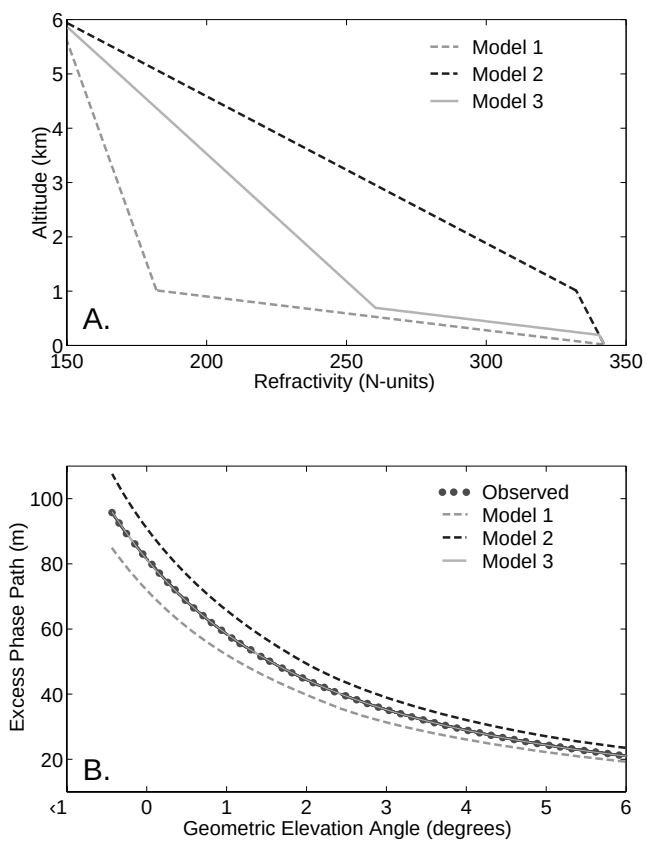

Figure 5. (a) Example models from a parameter search for refractivity structure. (b) Excess phase path ΔS versus geometric satellite elevation angle for the models shown in (a). Dots show measured ΔS^{GPS}, and are best fit by ΔS of Model 3.

San Diego area radiosonde data commonly exhibit critically to super-refractive gradients in the near-surface, particularly where warm, dry continental air masses cap the moist, cool marine boundary layer over the Pacific Ocean's California current. Refractivity gradients are normal within the marine boundary layer and above the mixing interface, and differ from CIRA+Q by < 3 RMS N-units above 6 km.

To determine the "best fit" model of ΔS^{GPS}, we perform a parameter grid-search over all $Z_A - Z_1$ and $Z_B - Z_A$ between 0 and 1 km with a 20 m increment (i.e., a total of 2500 different models of $N(Z)$). ΔS^{GPS} and ΔS^{mod} were compared using the L_2-norm (root-mean-square, or RMS) of the difference between the two. Figure 5 shows examples of refractivity models with differing Z_A and Z_B, and the corresponding ΔS^{mod} curves. Excess phase path can vary by tens of meters in the models investigated by the parameter search, so GPS measurements should provide significant constraint of atmospheric refractivity structure.

5. Results

Refractivity models that best fit the GPS excess phase path ΔS^{GPS} were compared to refractivity structure measured by radiosondes. Radiosonde data from two locales were used for comparison, including: (1) four high resolution Vaisala radiosondes ($\sim$20 m sampling at altitudes $<$6 km) released from the instrument pier on Point Loma; and (2) 377 VIZ soundings collected at $\sim$12 hour intervals from Marine Corps Air Station Miramar, located 20 km north-northeast of the GPS instrument (Figure 1). The latter were high resolution data that had been decimated to significant levels.

5.1. Comparison to Point Loma radiosondes

Plate 1 depicts modeling of ΔS^{GPS} measurements coincident with the four radiosondes launched from the instrument platform at Point Loma. Best-fit models of ΔS^{GPS} are shown as solid black lines, "envelopes" of models that fit to within 10 cm RMS difference are depicted as thin dashed black lines, and color contours indicate the minimum RMS misfit of ΔS^{GPS} from among all models that crossed a given point on the (N, Z) plane. The radiosonde refractivity (depicted as white circles) generally coincides with low RMS misfit $\|\Delta S^{\mathrm{GPS}} - \Delta S^{\mathrm{mod}}\|$. Moreover, in most cases (i.e., Plates 1a, 1b, and 1d), the model that best fits ΔS^{GPS} closely approximates the model that would best fit the radiosonde refractivity.

The refractivity model that best fits ΔS^{GPS} does not always match the radiosonde refractivity profile, however. In Plate 1c, the best fitting model has a large (~ 50 N-unit lapse) duct beginning at 700 m altitude. The radiosonde refractivity gradient is more variable than in other examples, but a model having a smaller duct at lower altitude would better match the observed radiosonde refractivity. However, the radiosonde profile mostly falls within the envelope of models that fit ΔS^{GPS} to within 10 cm RMS. The low-RMS envelope includes the entire range of modeled duct onset altitudes, from 0 to 1 km, so the difference between radiosonde and GPS estimates of refractivity in Plate 1c simply demonstrates that ground-based measurements of excess phase path do not always adequately constrain the altitude of anomalous refractive structures. Poor constraint of altitude is a manifestation of the ill-posed nature of the integral equation (3).

Ambiguity of the duct altitude is very apparent when the RMS misfit $\|\Delta S^{\mathrm{GPS}} - \Delta S^{\mathrm{mod}}\|$ is examined in parameter space. In Plate 2, RMS misfit is contoured as a function of duct onset altitude Z_A and the difference in refractivity across the duct $N_A - N_B$. The best fit models yield RMS misfit of between 3.2 and 8.3 cm, so other

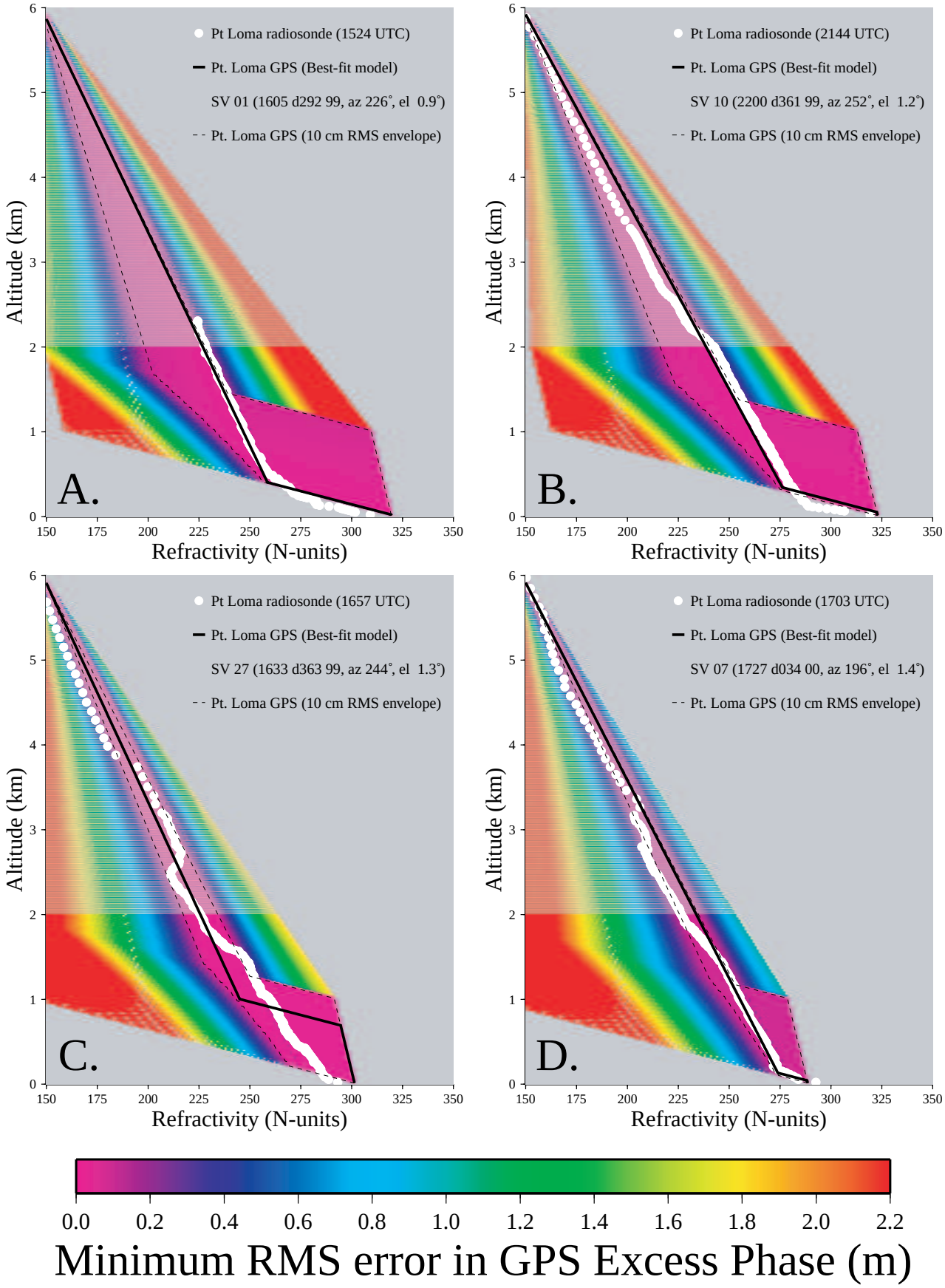

Plate 1. Refractivity versus altitude for the four radiosondes released from the instrument pier at Point Loma. White dots are radiosonde measurements, solid black line is the best fit model of contemporaneous ΔS^{GPS}, dashed black line is the envelope of models with less than 10 cm RMS error in ΔS^{GPS}, color denotes the minimum error in all models of ΔS^{GPS} at given (N, Z).

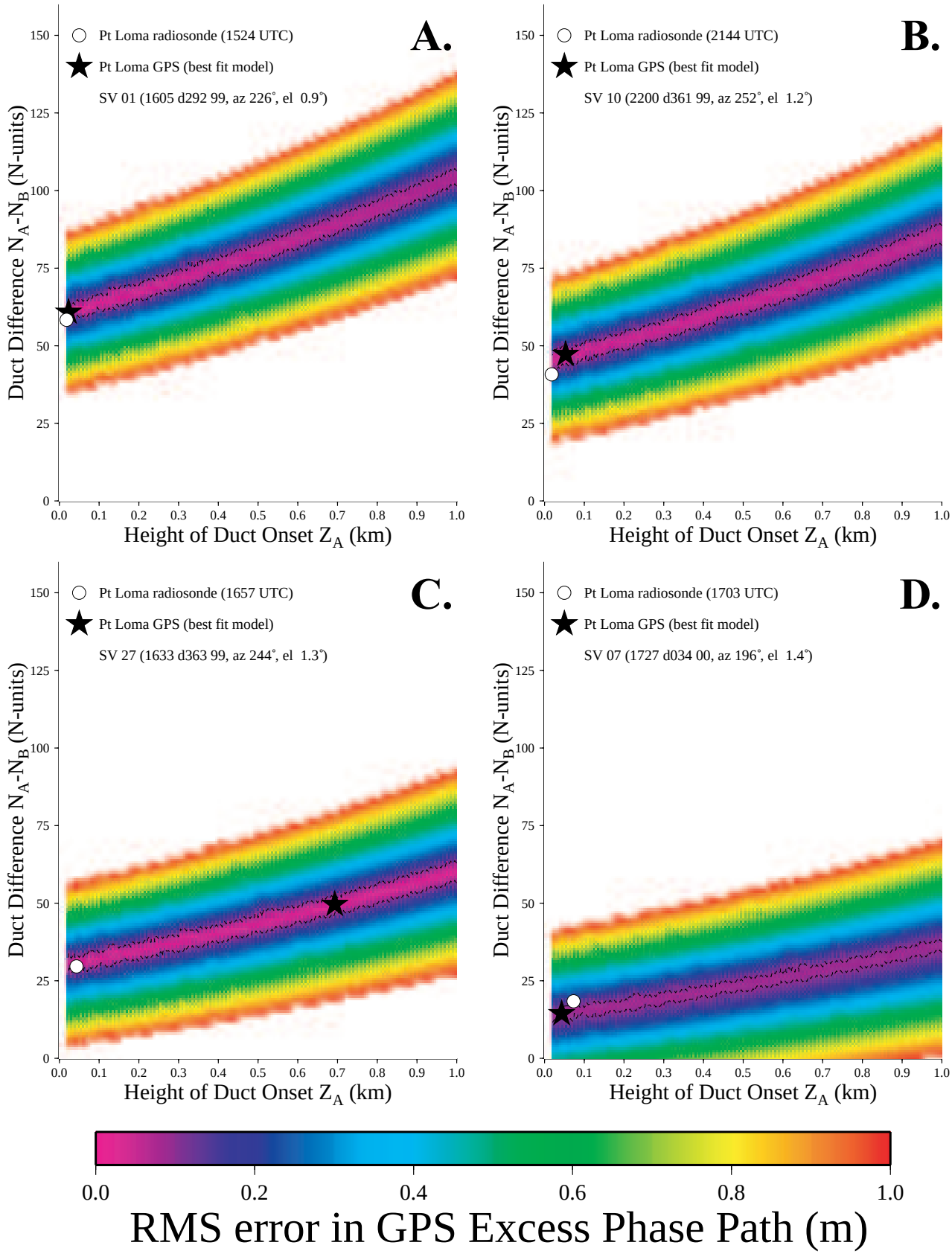

Plate 2. Parameter-space plots of results in Plate 1. Black star is the best fit model of ΔS^{GPS}; white dot is best fit model of radiosonde refractivity; color contours are RMS residual of the model of ΔS^{GPS}, with dashed black line denoting the 10 cm RMS contour.

Table 1. Individual error terms in GPS point positioning. Group I corresponds to parameters that are explicitly summed in the estimate of ΔS^{GPS}, Group II contains parameters that are implicit, and Group III includes non-parametric errors. Uncertainty sources: (1) Propagated from uncertainty of Met3 measurements; (2) Formal errors of parameter estimation; (3) Estimated from post-fit residuals; (4) Repeatability of network solutions for site coordinates; (5) *Zumberge et al.* [1997] errors for solutions from a 50 station network; (6) RMS of 3.5 cm amplitude modeled ocean multipath [*Sokolovskiy et al.*, 2001]; (7) Instrument noise for phase measurements in linear combination.

Error Contribution	Group	Zenith 1σ, cm	1° Elev 1σ, cm	Source
Dry Tropospheric Delay Parameters	I	0.0	3.4	(1)
Wet Tropospheric Delay Parameters	I	1.2	38.3	(2)
Inadequacy of Tropospheric Mapping Functions	I	0.0	∼200	(3)
Phase Ambiguity	II	4.0	4.0	(2)
Receiver Clock	II	0.5	0.5	(2)
Site Coordinates	II	1.6	0.5	(4)
Orbital Position	II	4.4	4.4	(5)
Satellite Clock	II	3.7	3.7	(5)
Multipath	III	2.5	2.5	(6)
Instrument Noise	III	0.3	0.3	(7)

models within the 10 cm envelope are not necessarily distinguished from the best fit at high confidence. The best fit model of ΔS^{GPS} on day 292 (black star in Plate 2a) is almost identical to the model that best fits the radiosonde refractivity (white circle), but other models with higher altitude onset of critical refraction and larger refractivity difference yield similar RMS misfit. Hence, coincidence of the best fit models of GPS and radiosonde in Plates 2a, 2b and 2d may be partially serendipitous.

5.2. Quantification of Error

There are several contributors to discrepancies between GPS and radiosonde estimates of atmospheric refractivity. Misfit between the two combines (1) true error in the estimate of ΔS^{GPS}; (2) true error in the radiosonde estimate of refractivity (from errors in the measurements of atmospheric properties P, T and ν, plus uncertainty in the empirical constants in relations (10)–(13)); (3) real differences in atmospheric conditions sampled at different locations and times; and (4) inadequacies of the mapping from ΔS^{GPS} to refractivity (e.g., the limited model space that was searched and the ill-posed integral operator in equation (3)). First we discuss the relative contributions of radiosonde and GPS measurement errors to estimates of excess phase path, and using those error estimates we infer some implications for atmospheric inhomogeneity.

5.2.1. Error in ΔS^{GPS}. To quantify error in the GPS measurement of excess phase path ΔS^{GPS}, it is useful to first separate the error into its

individual contributions. Table 1 lists separately all of the potential sources of error in estimates of tropospheric excess phase path between GPS satellite and antenna phase center, and quantifies those errors as standard deviations for a range at zenith and a range at $\sim 1^o$ elevation angle. To understand how these errors may combine in the estimate of tropospheric excess phase path, it is important to note that (1) the estimate of ΔS^{GPS} sums the elevation-mapped parameters we designated as "Group I" plus the residual of the Bernese parameter estimation; and (2) the sum of all the listed errors plus the residual must be zero.

The fact that errors in Table 1 must sum to zero when added to the residual places a firm upper bound on errors in the estimate of ΔS^{GPS}. For example, note that if errors in the estimate of tropospheric wet and dry delay (including errors in the assumed elevation mapping function) are expressed only in the post-fit residual, these terms will cancel resulting in no corresponding error in the estimate of ΔS^{GPS}. If on the other hand "Group I" error terms were perfectly cross-correlated with "Group II" errors, error in ΔS^{GPS} would include all of the error in estimation of the "Group I" terms plus the multipath and instrument noise (which are included because they are expressed in the phase residuals but are independent of the desired tropospheric excess phase path). Consequently, the worst case scenario for standard error in estimated ΔS^{GPS} would correspond to the RMS sum of the "Group I" plus "Group III" errors (at corresponding elevation), or the RMS sum of the "Group II" plus "Group III" errors, whichever is smaller. The upper bound error is the smaller of the two because "Group I" errors must be offset by "Group II" errors in order to generate an error in ΔS^{GPS}. Hence, the 95th percentile (2σ) error in estimates of ΔS^{GPS} is $\leq$15 cm (i.e., twice the RMS sum of "Group II" plus "Group III" errors).

Error will be even smaller if "Group II" errors mitigate each other (e.g., if orbit errors partially cancel satellite clock errors), or if they are expressed in the post-fit residual. Also, the "Group III" error terms are dominated by frequencies > 0.02 Hz which do not translate into significant errors in refractivity structure. Near-field multipath occurs at frequencies that can influence refractivity models however. Although the placement of the GPS antenna in this experiment (at the edge of a wooden pier— a poor microwave reflector— overhanging a 13 m drop to the ocean surface) argues against significant near-field reflection, we cannot rule out the possibility. We will revisit the topic of multipath error in a later section of this paper.

5.2.2. Error in ΔS^{Raob}. Error in radiosonde refractivity can propagate from both the empirically derived constants in equations (10)–(13) and from error in measurements of the atmospheric properties. *Thayer* [1974] estimates error in the regression constants in equation (10) to result in less than 0.05% error in N. Error in the regression constants will behave like a bias rather than a random error, and so would contribute a similar $< 0.05\%$ error to the estimate of excess phase path, ΔS^{Raob}. Hence, a typical ~ 100 m ΔS^{Raob} at $\beta = 1^o$ elevation would have < 5 cm of error contributed by the empirical constants.

Similarly, the components of radiosonde measurement error that can contribute significantly to error in ΔS^{Raob} are the bias terms. Older Vaisala radiosondes such as were used at Point Loma (manufactured in 1992) exhibit "dry bias" errors of 1–1.5 g kg^{-1} in measurement of moisture content as a result of gradual contamination of the humidity sensor by desiccants used in the radiosonde packaging [*Weckwerth et al.*, 1999]. This could generate up to 10% bias in estimated precipitable water vapor (PWV) which, on a global average ~ 15 cm zenith wet delay, would result in ∼50 cm underestimation of ΔS^{Raob} at 1° elevation angle. We corrected for the dry bias using an algorithm developed from extensive testing of time-, temperature- and humidity-dependent contamination of Vaisala humidity sensors [*Miller et al.*, 1999]. The correction changed the ΔS^{Raob} estimates by < 20 cm; much less than the 50 cm estimate above because humidity was quite low in these soundings. Relative

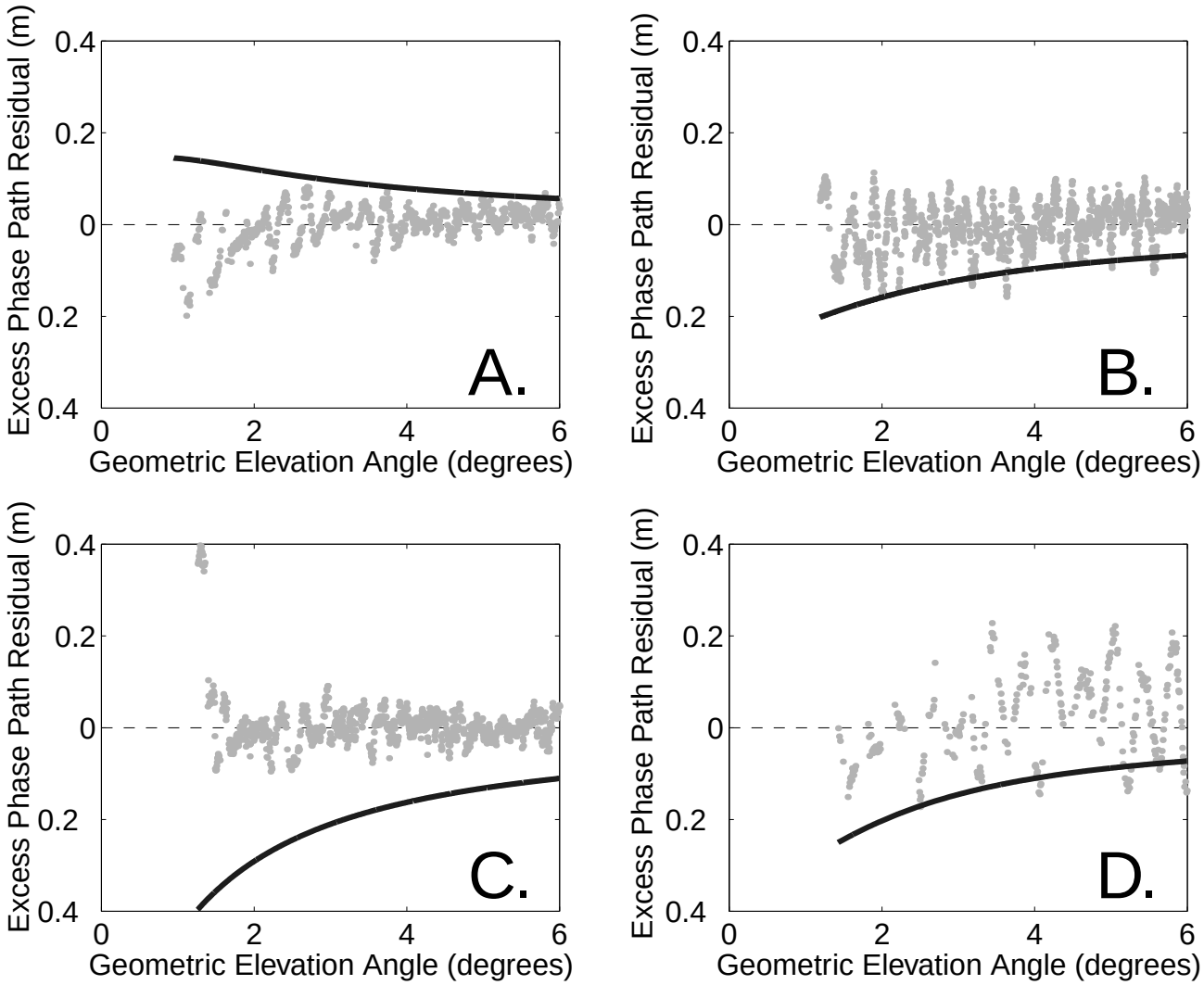

Figure 6. Excess phase path residuals. Gray dots are residuals of observed ΔS^{GPS} minus best fit models of same. Lines depict ΔS^{Raob} modeled from the radiosonde refractivity minus the best fit models of ΔS^{GPS}. Panels depict results corresponding to the similarly lettered panels of Plates 1–2.

humidity remains the most error-prone measurement after bias correction however: ν measurements by corrected radiosondes of this type are still subject to errors up to 3% of the measurement [e.g., *Yagi et al.*, 1996]. For the humidity conditions measured here, 3% bias error would introduce 6 cm of error in ΔS^{Raob} at 1° elevation angle. Other measurement errors have negligible effect, so the total error in estimates of ΔS^{Raob} should not exceed 16 ($= 2\sqrt{6^2 + 5^2}$) cm at 95% confidence, for elevation angles above 1°.

5.2.3. Sampling difference. An example of a real difference in sampled refractivity resulting from inhomogeneity can be seen in the difference between estimates of ground surface refractivity N_1 from the Vaisala radiosondes and the nearby meteorological sensor. Surface radiosonde measurements differ by 0.0 to 7.5 N-units from the meteorological sensor refractivity at the time of radiosonde launch, and by 3 to 10 N-units from the met sensor measurement at the time of GPS satellite rise or set. These differences exceed the 95% confidence on combined estimates of measurement error (5.5 N-units) and so must result from small-scale spatial inhomogeneities and temporal variability. $<$10 N-unit variability is not unreasonable for the scales of space-time separation on which the measurements were made (around 12 m and $<$ 40 minutes), particularly near the ground surface where boundary-layer effects tend to localize. Near-surface inhomogeneity is unlikely to influence GPS excess phase path significantly, however. For example, a 10 N-unit change in refractivity along a 100 m segment of path would change the excess phase path by just 1 mm.

Still, inhomogeneity of atmospheric properties can contribute significantly to differences between radiosonde and GPS estimates of refractive environment. GPS integrates atmospheric refractivity along a path nearly tangential to the Earth's surface while the radiosonde is an approximately vertical point-sampled profile; hence any lateral spatial variations will yield different estimates of excess phase path. We have estimated error in ΔS^{GPS} to be 15 cm at 95% confidence, and error in ΔS^{Raob} should not exceed 16 cm above $\beta = 1^o$. Hence, if atmospheric refractivity were truly spherically symmetric and time-invariant, the difference between GPS and radiosonde estimates of excess phase path would not exceed 22 cm at 95% confidence. The differences (shown as lines in Figure 6) between ΔS^{Raob} from Point Loma radiosondes and the best-fit models ΔS^{mod} of GPS measurements are as much as 40 cm. The largest difference $\Delta S^{\mathrm{Raob}} - \Delta S^{\mathrm{mod}}$ occurs in Figure 6c (corresponding to the comparisons in Plates 1c and 2c). Figure 6 also depicts (as dots) the residuals of the GPS-measured and best-fit modeled excess phase paths, $\Delta S^{\mathrm{GPS}} - \Delta S^{\mathrm{mod}}$. The residuals indicate that the simple model used in this study is adequate to parameterize virtually all of the ΔS^{GPS} signal at periods greater than a few minutes.

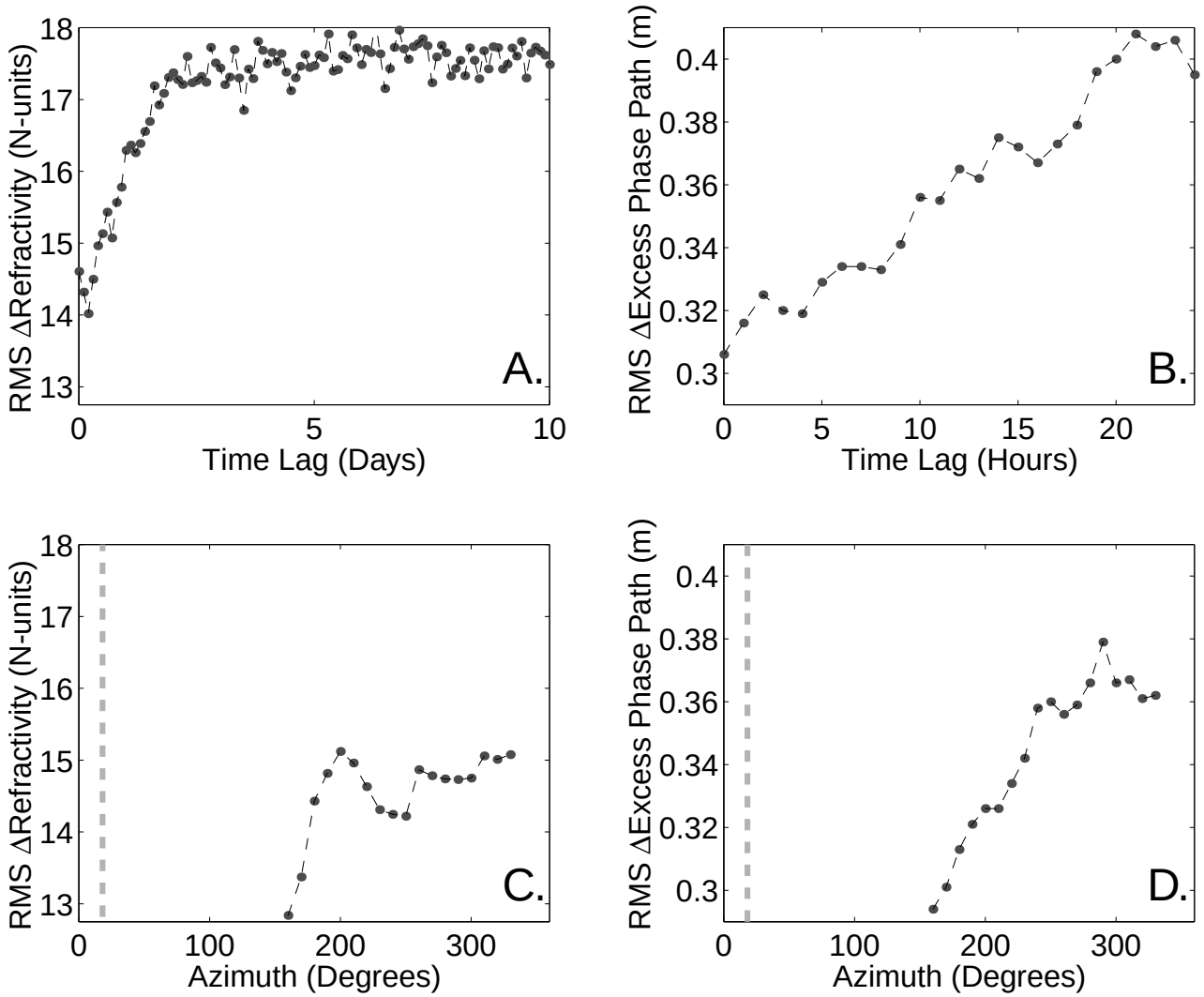

Figure 7. Comparison of GPS estimates of refractivity N and excess phase path ΔS to Miramar radiosonde measurements. (a) RMS of $N^{\mathrm{GPS}} - N^{\mathrm{Raob}}$ versus time lag. (b) RMS of $\Delta S^{\mathrm{GPS}} - \Delta S^{\mathrm{Raob}}$ versus time lag. (c) RMS of $N^{\mathrm{GPS}} - N^{\mathrm{Raob}}$ versus GPS azimuth. Dashed gray line is the azimuth to station Miramar. (d) RMS of $\Delta S^{\mathrm{GPS}} - \Delta S^{\mathrm{Raob}}$ versus GPS azimuth.

5.3. Comparison to Miramar radiosondes

During six months of the experiment we collected 3074 usable measurements of GPS excess phase path ΔS^{GPS}; over the same period, 377 radiosondes ($\sim$two per day) were released from an upper-air sounding station at Miramar Marine Corps Air Station. Miramar soundings use VIZ radiosondes, which do not exhibit the dry bias found in Vaisala humidity sensors. Miramar is about 20 km NNE of the GPS site (Figure 1), and so the atmosphere measured by radiosonde and GPS are likely to be even more dissimilar than for radiosondes released at Point Loma. Nevertheless, the large number of measurements permits us to compare GPS and radiosonde estimates of refractivity in a gross statistical sense.

Figure 7 compares Point Loma GPS and Miramar radiosonde estimates of refractivity (panels a, c) and excess phase path (b, d) as functions of time separation and GPS satellite azimuth. RMS difference in refractivity is the L_2-norm of the difference between radiosonde refractivity and the best-fit model of GPS excess phase path, $\|N^{\mathrm{Raob}} - N^{\mathrm{GPS}}\|$, summed over all radiosonde measurements below 6 km. RMS difference of the excess phase path compares ΔS^{GPS} with an estimate of ΔS^{Raob}, which is calculated from the integral of surface refractivity N_1 from the Point Loma meteorological sensor plus a linear interpolation to subsequent radiosonde observations.

Figure 7a shows RMS differences in refractivity, binned by time separation of the measurements. The minimum RMS difference occurs near $\Delta t = 0$ and the decorrelation time for refractivity estimates is about 2.5 days. The RMS 14 N-units of difference in contemporaneous measurements combines (1) "smoothing" of the complex vertical refractivity structure by our simple linear gradient model, (2) the ill-posed solution (i.e., uncertainty of the duct altitude) for refractivity from ground-based ΔS^{GPS}, and (3) spatial inhomogeneity of atmospheric refractivity. We calculated the difference between Miramar radiosonde refractivity and the model in the GPS search space that best fits that radiosonde refractivity in a least-squares sense. This calculation suggests that "smoothing" by the linear gradient model profile contributes about RMS 7.6 N-units of error, leaving about RMS 11.7 N-units from duct altitude uncertainty and spatial inhomogeneity. Figure 7b demonstrates that indeed a substantial portion of the refractivity difference must derive from spatial inhomogeneity: The RMS difference in excess phase path, $\|\Delta S^{\mathrm{GPS}} - \Delta S^{\mathrm{Raob}}\|$, is 30 cm for simultaneous measurements— hence too large to attribute to error in the GPS and radiosonde measurements.

Spatial inhomogeneity of refractivity is more difficult to characterize than temporal variability. In Figure 7c-d, we show the RMS differences of refractivity and excess phase path as a function of azimuth to the GPS satellite. GPS measurements are limited to western azimuths because local topography masks the horizon to the east (Figure 1), and the masked azimuths include everything within 50° of station Miramar. However there does appear to be a dependence, with GPS observations looking south to south-southeast ($160 - 180^o$) yielding results that are $\sim$7 RMS N-units and $\sim$20 RMS cm more similar to the radiosonde measurements than the westward-looking GPS observations. The GPS horizon is over land between $\sim$350–180° (Figure 1), implying that the atmosphere to the south over the coastline is more similar to the atmosphere sampled by Miramar radiosondes than is the atmosphere over the Pacific Ocean.

As with RMS refractivity, discrepancies between the GPS and radiosonde estimates of duct altitude, Z_A^{GPS} and Z_A^{Raob}, could result either from spatial inhomogeneity or from ill conditioning of the inverse mapping from excess phase path to refractivity structure. We have observed in Plate 2 that duct altitude is poorly constrained from ground-based ΔS^{GPS}. However, ΔS^{GPS} does contain information about the altitude of ducting. The difficulty arises because the diagnostic signal occurs at very low satellite elevation angles, as illustrated graphically in Figure 8. Refractivity models A and B in Figure 8a have identical excess phase path at zenith, but very different duct onset altitudes. The excess phase path from these two models differs significantly only at the lowest satellite elevation angles, reaching $\sim$10 cm at about $\beta = 2^o$ (Figure 8b). At extremely low elevation angles, the difference can be quite large (e.g., 1.6 m at -0.4^o satellite elevation in the example shown).

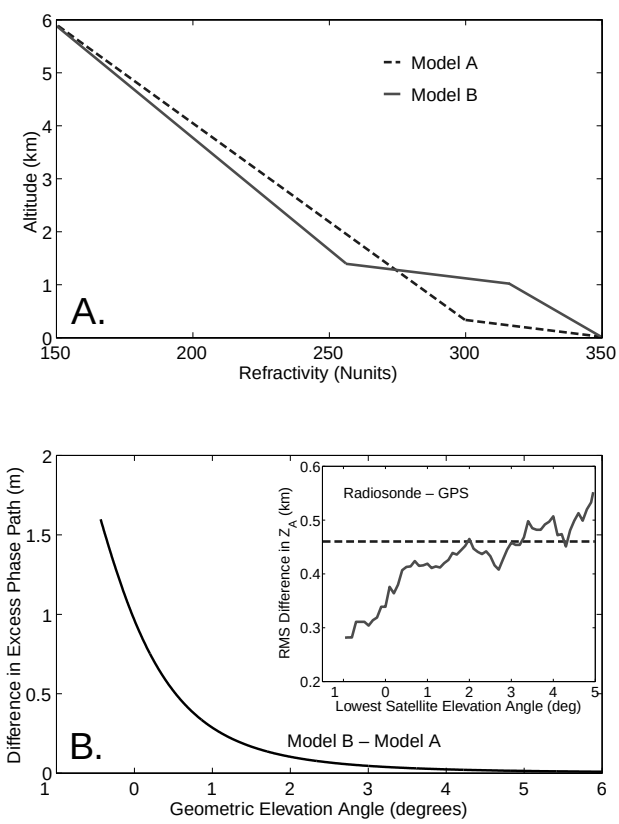

Figure 8. Duct altitude and excess phase path ΔS. (a) Two refractivity models with different duct altitudes but identical zenith ΔS. (b) Difference in ΔS of the two models at low elevation angles. Inset: RMS difference of duct onset altitudes predicted from ΔS^{GPS} and from Miramar radiosondes, versus minimum satellite elevation angle. Dashed line is the relationship expected if estimates are completely uncorrelated.

Unfortunately, in the data presented here, clean measurements are rarely available at the very lowest elevation angles. About 22% of all GPS satellite rises and sets yielded usable observations below 2° satellite elevation angle, and only 0.9% produced reliable estimates of ΔS^{GPS} below zero. Hence, while the elevation dependence of ΔS^{GPS} would theoretically permit us to distinguish the onset altitude of ducts, in practice the onset altitude of ducting is rarely well-resolved.

In the inset of Figure 8b we compare Z_A^{GPS} of the best fit model of ΔS^{GPS} to Z_A^{Raob} of the model that best fits the contemporary Miramar radiosonde. To determine what the RMS difference would be if the two estimates were completely uncorrelated, we also compared Z_A^{Raob} to a set of randomly-generated, Poisson-distributed numbers between 0 and 1 km. The artificial data set produced an RMS difference of $\sim$0.44 km. Estimates of Z_A^{GPS} in which the lowest satellite elevation angle of the ΔS^{GPS} measurement is $\gtrsim 1.5^o$ similarly have $\|Z_A^{\mathrm{Raob}} - Z_A^{\mathrm{GPS}}\| \gtrsim 0.44$ km. The RMS difference improves for GPS observations below 1.5^o, dropping to about 0.3 km for GPS measurements tracked below 0° geometric elevation angles. Of course, the GPS and radiosonde estimates of Z_A are separated by more than 20 km and up to 6 hours in time, so the misfit combines the limitations of modeling ΔS^{GPS} with sampling differences. Nevertheless, it is clear that estimates of duct altitude benefit significantly from measurements at extremely low satellite elevation angles.

Plates 1 and 2 suggest the change in refractivity or "lapse" across a duct is relatively well-determined, to within limits imposed by uncertainty of the duct altitude. To evaluate the GPS estimate of duct lapse, we limited the model search space to ducts with zero onset altitude. Forcing the model to fit a surface duct yields a conservative estimate of duct lapse, as implied for example in Plate 2. A time series comparison of this "minimum-lapse" model of ΔS^{GPS} to models of Miramar radiosonde refractivity is plotted in Figure 9a. Here, black dots indicate refractivity at the ground surface N_1 measured by the meteorological sensor at times of GPS remote sensing. N_1 of the best fit models of Miramar radiosondes (the tops of the thin, light gray bars) is similarly fixed to the Point Loma met sensor measurements. The gray dots represent refractivity N_B at altitude Z_B^{GPS} (i.e., the top of ducting for the surface duct model of ΔS^{GPS}). The best fit model of Miramar radiosonde refractivity has variable duct onset altitude Z_A^{Raob}, as shown in Figure 9b, and refractivity at Z_B^{Raob} corresponds to the base of the thin gray bars in Figure 9a. The GPS estimate of N_B compares favorably with the radiosonde much of the time, with larger misfit occurring when ducts are elevated. The RMS difference in duct lapse (14.5 N-units) is much smaller than the time-variability (standard deviation 23.8 N-units).

6. Discussion/Conclusions

Our estimates of potential error in the GPS excess phase path (Table 1) include an estimated ~ 2.5 cm RMS contribution from a 3.5 cm amplitude multipath error. The latter is based on a simplified model of multipath introduced by reflections off the ocean surface at the site [*Sokolovskiy et al.*, 2001] and assumes negligible reflection from other sources. Other multipath is of course possible, but for multipath in the GPS excess phase path to approach even a single wavelength of the GPS linear combination (~ 10.8 cm) would require a highly unlikely degree of constructive interference from a large number of reflective sources. One can evaluate the phase multipath environment by averaging postfit residuals, and in Figure 10a we show the average of all 3000+ elevation-dependent residuals from the best-fit models of refractivity structure. The figure

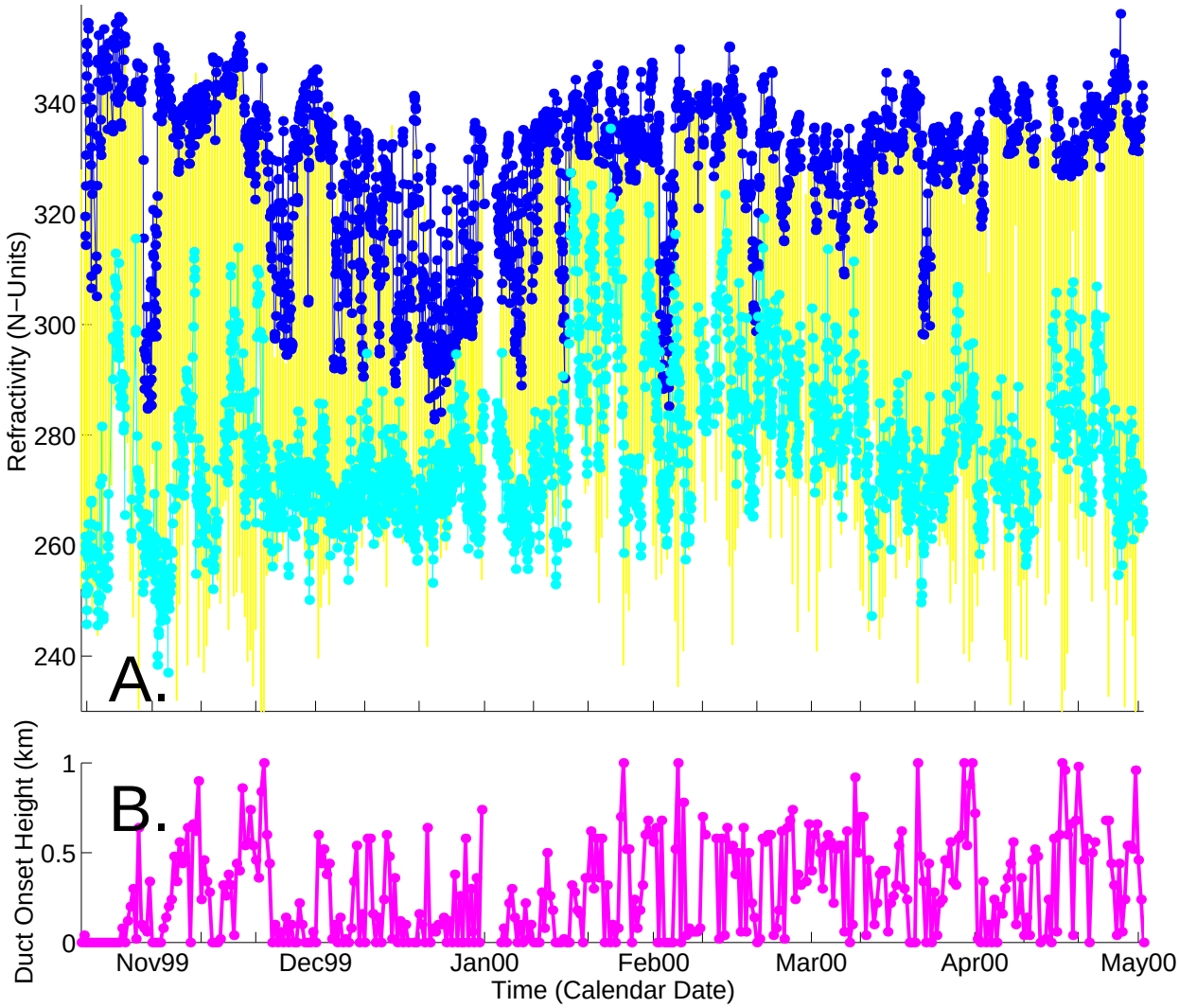

Figure 9. Time series comparison of GPS and radiosonde estimates of duct lapse. (a) Refractivity time series. Blue dots are refractivity at Point Loma meteorological sensor at times of ΔS^{GPS} measurements; top of thin yellow bars are met sensor refractivity at times of Miramar radiosonde release. Cyan dots are refractivity at the top of ducting N_B for the best fit surface duct model of ΔS^{GPS}, and bottom of thin yellow bars denote the top of duct for a model that best fit the radiosonde refractivity. (b) Height of duct onset for best fit model of radiosonde refractivity.

also depicts one example of averaging from a single satellite; in all cases the averages for a single satellite and for all satellites are quite similar above 1° elevation. The mean residuals manifest a ~ 3.5 cm amplitude high-frequency error that is very consistent with the predicted ocean multipath above 1° elevation, but appear to indicate an even higher frequency (and larger amplitude) error below 0.5^o elevation. This reflective source must be even further away than the ocean surface, and may be a constructive interference pattern from guided wave phenomena in atmospheric ducts over the ocean.

There is also a low-frequency signal apparent in these averages, which could be attributed to either multipath from a near-field source or to a bias error introduced by the simple linear model of refractivity used in this study. The mean of differences between best-fit models of ΔS^{GPS} and Miramar radiosondes (Figure 10b) suggests there is a refractivity bias error, resulting from the tendency for refractivity to follow an exponential rather than linear function of altitude. However, ray modeling of this refractivity bias (the light gray line in Figure 10a) yields an excess phase path bias that differs significantly from the observations between 0–3° satellite elevations. Hence, the low-frequency component of the mean residual most likely represents near-source multipath. Nevertheless, the contribution of multipath error to estimates of ΔS^{GPS} is approximately equal to our model-based estimate: The RMS of the mean of the residuals shown in Figure 10a is 2.49 cm.

GPS sensing of atmospheric refractivity structure has a large array of potential applications. Applications to communications and radar target acquisition were discussed in the introduction, but other potential venues include weather-sensing (e.g., imaging of the water vapor distribution in storm systems) and assimilation of the excess phase path integral into numerical weather forecast models. GPS-derived refractivity structure could also be used to improve corrections for atmospheric effects in other space-geodetic applications, e.g., interferometric synthetic aperture radar (InSAR).

Estimation of the vertical refractivity profile from a single ground-based GPS site clearly has limitations, however. Relatively poor constraint of the altitude of refractory structures evidenced in this study would limit the utility of GPS for some purposes. Poor altitude resolution is an unavoidable consequence of the source-receiver geometry, and will not be easily overcome when the GPS receiver is on the ground. Other commonly-used observables such as Doppler shift actually have less information content than the excess phase path used in this analysis, and while GPS waveform

(amplitude) data may offer additional informational constraint, it will require significant adaptation of existing instrumentation to be useful. Ultimately, the best way to overcome the limited height resolution of ground-based GPS will be to use crossing rays from multiple sites in a tomographic inverse approach. However, the method for refractivity profiling that we have described is somewhat rudimentary, and there is substantial room for improvement even for profiling from a single site. We identify two ways to improve upon these results: (1) more robust parameterization of the data, and (2) better acquisition of excess phase path measurements at low elevation angle.

Equation (3) describing the excess phase path is an example of a Fredholm integral equation of the first kind, and the solution of such is unstable in the presence of observational error [*Twomey*, 1996]. The robust approach to solving ill-posed problems is to limit the solution space. Recognizing this, we used a skeletalized *ad hoc* parameterization of the refractivity profile and solved a least squares minimization in the limited discrete space of the parameters. The goal of this parameterization was to characterize the surface ducting conditions which commonly affect radio wave propagation in coastal regions. However, despite limiting the solution space to two bounded parameters, our model includes one variable parameter (the duct onset altitude Z_A) which is poorly constrained and highly cross-correlated with the other. However, several alternative regularization methods could be used to better delimit the inversion for refractivity structure [see, e.g., *Tikhonov and Arsenin*, 1977]. *Gaikovich and Sumin* [1986] used two different regularization techniques to reconstruct vertical refractivity profiles from simulated astronomical refraction data, and obtained better performance using the stochastic properties of atmospheric refractivity to guide the inversion. Ideally, correlation between model parameters should be minimized by expansion into a series of empirical orthogonal functions (EOFs). This approach requires *a priori* information about the parameter probability density distribution, e.g., a vertical covariance matrix of refractivity. In effect, one would need a large ensemble of *in situ* refractivity profiles with sufficiently high resolution to characterize the full statistics of refractivity (including dependence on location and seasonal variation). Such information was not available for this study, but regularization and expansion to EOFs would both decrease the bias error in refractivity profiles and minimize intersection with the solution null space relative to the method we used here.

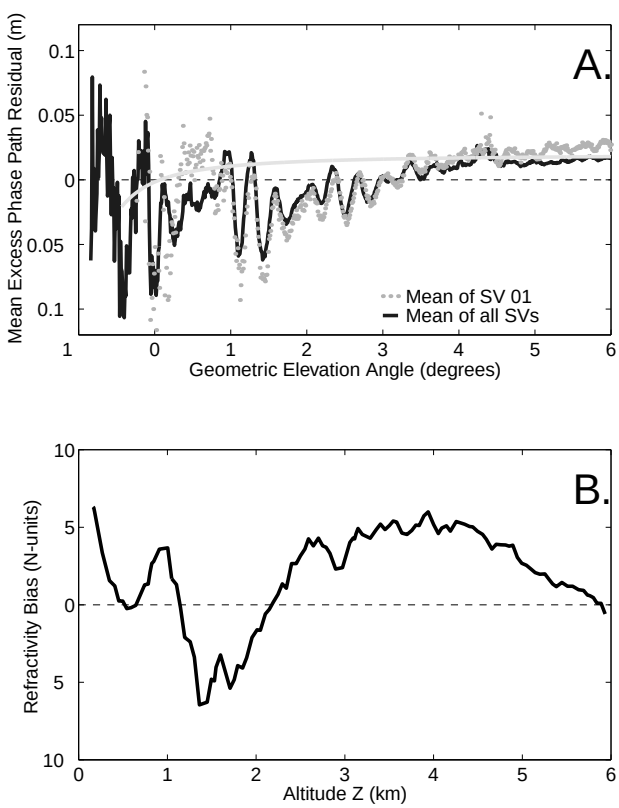

Figure 10. (a) Means of residuals from modeling of GPS excess phase path measurements. Black line is the mean of all satellites; gray dots are the mean of SV01; the light gray line is a ray model of atmospheric refractivity bias inferred from the mean refractivity difference between best-fit models of ΔS^{GPS} and Miramar radiosondes, shown as a function of altitude in (b).

GPS estimates of the altitude of refractory structures clearly benefit from excess phase path measurements at very low satellite elevation angles ($< 1^o$). Less than 1% of the GPS satellite rises and sets in this data set yielded reliable excess phase path measurements below 0° elevation angle, but in about 25% of all cases the receiver was able to track the satellite below 0°. Few of the lowest-angle measurements were successfully modeled because (1) most low-angle phase observations were rejected by the algorithm used for preliminary cycle slip detection and cleaning prior to GPS parameter estimation, and (2) the refractivity modeling algorithm rejected many more profiles containing low elevation angle observations because the RMS residual of the best fit model exceeded 12 cm. (Large RMS residuals were generally associated with unfixed cycle slips or misestimated ambiguities in short data segments, so these were culled from the data set). Improvement of the preprocessing algorithms would increase the number and quality of low-angle estimates of GPS excess phase path, and so improve vertical resolution of the refractivity structure. Improved instrumentation, such as receiver tracking algorithms with better low-angle performance or directed high-gain antennas, would reduce measurement gaps and cycle slips and further improve constraint of vertical refractivity.

Despite limited vertical resolution, ground-based GPS measurements provide useful constraint of atmospheric refractivity structure. Refractivity estimated from ΔS^{GPS} predicts nearby radiosonde refractivity better than would an average or reference model (e.g., CIRA+Q). The estimate of duct lapse, for example, is quite robust. And while some of the difference between GPS and radiosonde derives from limitations of the inverse method, a significant portion represents spatial inhomogeneity of atmospheric properties. The effects of spatial inhomogeneity are least ambiguous in excess phase path. Differences of RMS 10-20 cm between GPS measurements and Point Loma radiosondes result mostly from the difference between vertical sampling by the radiosonde versus quasi-horizontal integration by the GPS path. The RMS 30 cm difference between GPS measurements of excess phase path and Miramar radiosondes requires even larger sampling differences. Given the variability of atmospheric refractivity, future attempts to validate GPS sensing should attempt to minimize the spatial and temporal separation between GPS and *in situ* measurements.

Acknowledgments. Teresa Van Hove, John Braun and Jim Johnson of UCAR GST all contributed significantly to the development of processing algorithms used to estimate GPS excess phase path for this paper. Jim, along with Dave Mencin, also aided with the continuous site implementation. We thank Hal Cole and Junhong Wang of NCAR ATD for their help with correction of the radiosonde dry bias. The paper was improved by the suggestions of two anonymous reviewers. Some of the figures were generated using GMT [*Wessel and Smith*, 1998]. This research is sponsored by the Office of Naval Research, Dr. Scott Sandgathe, Code 322MM.

References

Anderson, K.D., Tropospheric refractivity profiles inferred from low-elevation angle measurements of Glob-al Positioning System (GPS) signals, *AGARD Conf. Proc., 567*, 1-6, 1994.

Azizov, A.A., K.P. Gaikovich, S.S. Kashkarov, and M.B. Chernyaeva, Determination of atmosphere parameters using navigation satellite signals, *Radiophys. Quant. Elec., 41*, 737-751, 1998.

Baumgartner, G.B., Hitney, H.V., and Pappert, R.A., Duct propagation modeling for the Integrated Refractive Effects Prediction System (IREPS), *Proc. Inst. Elec. Eng., 130*, 630-642, 1983.

Born, M., and E. Wolf, *Principles of Optics*, Pergamon Press, New York, 856pp., 1964.

Budden, K.G., *The Propagation of Radio Waves: The Theory of Radio Waves of Low Power in the Ionosphere and Magnetosphere*, Cambridge Univ. Press, New York, 669pp., 1985.

Fjeldbo, G., and V.R. Eshleman, The bistatic radar occultation method for the study of planetary atmospheres, *J. Geophys. Res., 70*, 3217-3225, 1965.

Fjeldbo, G., and V.R. Eshleman, The atmosphere of Mars analyzed by integral inversion of the Mariner 4 occultation data, *Planet. Space Sci., 16*, 1035-1059, 1968.

Fjeldbo, G., A.J. Kliore, and V.R. Eshleman, The neutral atmosphere of Venus as studied with the Mariner 5 radio occultation experiments, *Astron. J., 76*, 123-140, 1971.

Freehafer, J.E., Tropospheric refraction, in *Propagation of Short Radio Waves*, edited by Kerr, D.E., McGraw-Hill, New York, pp 9-22, 1951.

Gaikovich, K.P., and M.I. Sumin, Reconstruction of the altitude profiles of the refractive index, pressure, and temperature of the atmosphere from observations of astronomical refraction, *Izv. Atm. Oceanic Phys., 22*, 710-715, 1986.

Hitney, H.V., and J.H. Richter, Integrated refraction effects prediction system (IREPS), *Nav. Eng. J., 88*, 257-262, 1976.

Hitney, H.V., J.H. Richter, R.A. Pappert, K.D. Anderson, and G.B. Baumgartner, Jr., Tropospheric radio propagation assessment, *Proc. IEEE, 73*, 265-283, 1985.

Hopfield, H.S., Two-quadratic tropospheric refractivity profile for correcting satellite data, *J. Geophys. Res., 74*, 4487-4499, 1969.

Kirchengast, G., J. Hafner, and W. Poetzi, The CIRA86a Q_UoG model: An extension of the CIRA-86 monthly tables including humidity tables and a Fortran95 global moist air climatology model, IMG/UoG Technical Report for ESA/ESTEC, No. 8, 1999.

Kursinski, E.R., G.A. Hajj, K.R. Hardy, J.T. Schofield, and R. Linfield, Observing Earth's atmosphere with radio occultation measurements, *J. Geophys. Res., 102*, 23,429-23,465, 1997.

Miller, E.R., J. Wang and H.L. Cole, Correction for dry bias in Vaisala radiosonde RH data, in *Proceedings of the* 9th *Atmospheric Radiation Measurement (ARM) Program Science Team Meeting*, San Antonio, Texas, March 22-26, 1999.

Niell, A.E., Global mapping functions for the atmosphere delay at radio wavelengths, *J. Geophys. Res., 101*, 3227-3246, 1996.

Owens, J.S., Optical refractive index of air: dependence on pressure, temperature, and composition, *Appl. Opt., 6*, 51-58, 1967.

Rocken, C., R. Anthes, M. Exner, D. Hunt, S.V. Sokolovskiy, R. Ware, M. Gorbunov, W. Schreiner, D. Feng, B. Herman, Y.H. Kuo, and X. Zou, Analysis and validation of GPS/MET data in the neutral atmosphere, *J. Geophys. Res., 102*, 29,849-29,866, 1997.

Rothacher, M., and L. Mervart (Eds.), Bernese GPS Software Version 4.0, Astronomical Institute Unversity of Berne, Berne, Switzerland, 1996.

Sokolovskiy, S.V., C. Rocken, and A.R. Lowry, The use of GPS for estimation of bending angles of radio waves at low elevations, *Radio Sci., 36*, 473-482, 2001.

Spilker, J., GPS signal structure and performance characteristics, *J. Inst. Navi., 25*, 121-146, 1978.

Thayer, G.D., An improved equation for the radio refractive index of air, *Radio Sci., 9*, 803-807, 1974.

Tikhonov, A.N., and V.Y. Arsenin, *Solutions of Ill-Posed Problems*, John Wiley, New York, 258pp, 1977.

Twomey, S., *Introduction to the Mathematics of Inversion in Remote Sensing and Indirect Measurements*, Dover, Mineola, New York, 243pp., 1996.

Vasilenko, N.A., K.P. Gaikovich, and M.I. Sumin, Determination of atmospheric temperature and pressure profiles from astronomical refraction measurements near the horizon, *Izv. Atm. Oceanic Phys., 22*, 798-804, 1986.

Weckwerth, T.M., V. Wulfmeyer, R.M. Wakimoto, R.M. Hardesty, J.W. Wilson, and R.M. Banta, Meeting summary: NCAR-NOAA lower-tropospheric water vapor workshop, *Bull. Am. Meteo. Soc., 80*, 2339-2357, 1999.

Wessel, P., and W. H. F. Smith, New, improved version of Generic Mapping Tools released, it EOS Trans. Amer. Geophys. U., 79(47), 579, 1998.

Yagi, S., A. Mita and N. Inoue, WMO international radiosonde comparison – Phase IV; Final report, *World Met. Org. Instr. Obs. Meth. Rep. Ser., 59*, 1996.

Zuffada, C., G.A. Hajj, and E.R. Kursinski, A novel approach to atmospheric profiling with a mountain-based or air-borne GPS receiver, *J. Geophys. Res., 104*, 24,435-24,447, 1999.

Zumberge, J.F., M.B. Heflin, D.C. Jefferson, M.M. Watkins, and F.H. Webb, Precise point positioning for the efficient and robust analysis of GPS data from large networks, *J. Geophys. Res., 102*, 5005-5017, 1997.

Zumberge, J.F., M.M. Watkins, and F.H. Webb, Characteristics and applications of precise GPS clock solutions every 30 seconds, *Navigation: J. Inst. Nav., 44(4)*, 449-456, 1998.

(Received July 20, 2000.)